Rigid block coupled with a 2 d.o.f. system: Numerical and experimental investigation

Stefano Pagliaro[a], Angelo Aloisio[b], Rocco Alaggio[c] and Angelo Di Egidio[*]

DICEAA - University of L'Aquila, via G. Gronchi, 18-67100 L'Aquila, Italy

Abstract.   In this paper the linear elastic coupling between a 2 degree of freedom shear-type frame system and a rigid block is analytically and experimentally investigated. As demonstrated by some of the authors in previous papers, it is possible to choose a coupling system able to guarantee advantages, whatever the mechanical characteristics of the frame. The main purpose of the investigation is to validate the analytical model. The nonlinear equations of motion of the coupled system are obtained by a Lagrangian approach and successively numerically integrated under harmonic and seismic excitation. The results, in terms of gain graphs, maps and spectra, represent the ratio between the maximum displacements or drifts of the coupled and uncoupled systems as a function of the system's parameters. Numerical investigations show the effectiveness of the nonlinear coupling for a large set of parameters. Thus experimental tests are carried out to verify the analytical results. An electro-dynamic long-stroke shaker sinusoidally and seismically forces a shear-type 2 d.o.f frame coupled with a rigid aluminium block. The experimental investigations confirm the effectiveness of the coupling as predicted by the analytical model.

Keywords: elastic coupling; rigid block; gain coefficients and maps; experimental investigation

1. Introduction

Several papers have been dedicated to the comprehension of the behaviour of rigid block systems, starting from the pioneering work of Housner (1963). Both the seismic excitation (Yim *et al*. 1980, Pompei *et al*. 1998, Taniguchi 2002, Psycharis *et al*. 2013) and other kinds of ground excitation, such as harmonic or impulsive one-sine excitation (Spanos and Koh 1984, Zhang and Makris 2001, Kounadis 2013, Vassiliou *et al*. 2014) and random excitation (Spanos and Koh 1986) were considered.

Several papers presented general formulations for the rocking and slide-rocking motions of free-standing symmetric rigid blocks (Andreaus 1990, Shenton and Jones 1991, Voyagaki Ioannis *et al*. 2013, Shenton 1996, Tung 2007) performed the analysis of the different phases of motions by defining criteria for the transition between them. Some papers consider either non-symmetric rigid blocks (Contento and Di Egidio 2009, Dar *et al*. 2018), or three-dimensional blocks (Zulli *et al*.

---

[*]Corresponding author, Associate Professor, E-mail: angelo.diegidio@univaq.it
[a]Ph.D. Student, E-mail: stefano.pagliaro@graduate.univaq.it
[b]Ph.D. Student, E-mail: angelo.aloisio@graduate.univaq.it
[c]Associate Professor, E-mail: rocco.alaggio@univaq.it

2012, Di Egidio *et al*. 2014b, 2015). Other papers investigated the dynamics of rigid blocks in a general way (DeJong and Dimitrakopoulos 2014), whereas Kounadis (2014, 2015) focuses on the rocking instability (overturning) of different rigid block systems. Spanos *et al*. (2017) carried out an interesting experimental investigation of a block on a non-linear deformable foundation, while Aloisio *et al*. (2019a, b, 2020) identified the actual behaviour of a rocking masonry facade under seismic excitation using a linear regression approach.

Recently, many papers examined the coupling of the block with different passive or active devices in order to protect them from the overturning. For example, the effectiveness of base anchorages was studied in Makris and Zhang (2001), Dimitrakopoulos and DeJong (2012) in order to protect rigid blocks from overturning, whereas Di Egidio and Contento (2009, 2010), Contento and Di Egidio (2014), Calio and Marletta (2003), Vassiliou and Makris (2012), DeJong and Dimitrakopoulos (2014) highlighted the efficiency of the base-isolated system. Other types of passive control methods for the protection of rigid blocks were considered, for example, in Corbi (2006), where the authors proposed a sloshing water damper. A mass-damper dynamic absorber in the shape of a pendulum was used by different authors (Collini *et al*. 2016, Brzeski *et al*. 2016, de Leo *et al*. 2016, Di Egidio *et al*. 2019c, a), who demonstrated the general effectiveness of this kind of protection device. Instead, in Simoneschi *et al*. (2017a, b), Di Egidio *et al*. (2018) a mass-damper modelled as a single degree of freedom and running on the top of the block was considered as safety device. In Contento *et al*. (2019, 2017) a probability model to compare the effectiveness of base isolation and pendulum mass-damper in seismic protection of rigid block-like structures was proposed.

Also, active or semi-active devices were used to improve the dynamic and seismic performances of blocks. For example, Ceravolo *et al*. (2016, 2017) studied the use of semi-active anchorages using feedback-feedforward or feedback strategies to increase the acceleration required to topple a reference block. Recently Di Egidio *et al*. (2014a), Simoneschi *et al*. (2018), Di Egidio *et al*. (2020a) used an active control technique to increase the amplitude of base excitation able to topple a rigid block.

An interesting topic that is increasingly present in the scientific literature regards the dynamic improvement of structures by coupling them with devices of same or different type. In this field some papers Ormeo *et al*. (2012), Khatiwada *et al*. (2013), Huang *et al*. (2013), Muratovi and Ademovi (2015) represent an example. Specifically, in Huang *et al*. (2013), Muratovi and Ademovi (2015) particular attention was devoted to the coupling between a frame structure and a rocking block. The use of rocking rigid block as a protecting device of other kinds of structure represents a particular issue, not frequently dealt with. In papers Wada *et al*. (2011), Grigorian and Grigorian (2015) rocking walls are used to improve the dynamic and seismic response of existing buildings. In particular base pinned rocking wall are rigidly connected to the frame structure and provide a reduction of drifts, and suitable supports for energy-dissipating devices. In some recent works (Aghagholizadeh and Makris 2018, Makris and Aghagholizadeh 2017) the authors investigated a rigid coupling between a frame and a rocking wall under seismic excitations, mainly focusing on the differences between base pinned and base rocking rigid blocks. On the contrary, in Di Egidio *et al*. (2019d, b) a visco-elastic connection was considered. These papers showed that the rocking wall could act as a tuned mass damper for the frame if the coupling is correctly designed. It was assumed that multi-storey frames could be modelled through a dynamically equivalent 2 d.o.f. system like in Fabrizio *et al*. (2017b, 2019, 2017a). The effectiveness of such a visco-elastic connection was investigated by performing a numerical parametric analysis on mechanical systems representing real buildings. In more recent paper Di Egidio *et al*. (2020b), the seismic performance of visco-elastic

coupling of real frame structures and rocking walls has been investigated and physically interpreted.

This paper investigates the numerical and experimental behaviour of a 2 d.o.f. shear-type frame structure, elastically coupled with a rigid aluminum block. The work is conducted under the following assumption: it is possible to arrange a coupling system able to ensure benefits, whatever are the mechanical properties of the frame (Di Egidio *et al*. 2019d, 2020b). The primary purpose of the investigation is the validation of the analytical model. The system under test is not intended to represent any real structure. A Lagrangian approach leads to nonlinear equations of motion of the coupled-system. They are numerically integrated to investigate the response of coupled system. A parametric analysis leads to gain graphs, maps and spectra. They show the ratio between the maximum displacements or drifts of the coupled and uncoupled systems as a function of the system's parameters. Such graphs, maps and spectra allow an immediate understanding of the effects of the block: it has a beneficial effect when the ratio of displacements is less than unity. Experimental simulations verify the effectiveness of such coupling. A shear-type 2 d.o.f frame elastically coupled with a rigid aluminum block is harmonically and seismically driven by an electrodynamic long-stroke shaker. The systems response, in terms of displacements, measured by no-contact and optical/laser sensors, is post-processed using the software MATLAB® and Mathematica®. Then, both experimental and theoretical results are compared.

2. Motivation of the study

In this paper, experimental tests aim to validate the analytical model. In fact, the description of motion of a stand-alone rigid block is a bit difficult with classical analytical models, due to particularity of rocking motion. Although the classical Housner's model (Housner 1963) is able to represent correctly the main nonlinear characteristics of the rocking motion of a block, many other models that refine Housner's model were proposed in order to better describe the impacts of block with base support and the loss of energy occurring at each impact (Sorrentino *et al*. 2011, Ther and Kollar 2016, Kalliontzis *et al*. 2016).

The results of an analytical modelling show that coupling can achieve good performances in improving the dynamical behaviour of a frame. Nevertheless, as mentioned above, the model of Housner can represent correctly only the main characteristics of rocking motion, therefore the analytical and experimental behaviour could be slightly different. It is of fundamental importance to check whether the small differences between the ideal and real behaviour of block are able to change in a negative way the results provided by the analytical models. Consequently, an experimental validation of the analytical model is needed.

3. Analytical and experimental model

Both the analytical and experimental models refer to the same mechanical system. A shear-type 2-d.o.f frame is coupled with a rigid rocking block using a linear elastic device, which connects the first storey of the frame to a point on the vertical side of the block. The block has a mass $M=\rho \times 2b \times 2h_b \times s$, where $\rho=2450$ kg/m^3 (aluminium) and s is the dimension orthogonal to the plane of the figure. Fig. 1 shows the geometrical configuration and characteristics of the coupled mechanical system.
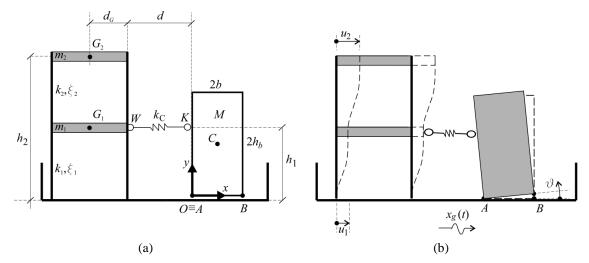
Fig. 1 Mechanical system: (a) Geometrical characterization of the system; (b) Lagrangian parameters u_1, u_2, ϑ (positive directions)

3.1 Analytical model

It is assumed that the block cannot slide and cannot undergo to free-flight motion, therefore only rocking motions can occur. Consequently, three Lagrangian parameters fully describe the motion. Such parameters are the displacements (relative to the ground) of the 2 d.o.f. system u_1 and u_2, and the rotation of the block ϑ. Figure 1b shows the positive directions of the three Lagrangian parameters. Two sets of three equations of motion, which describe the motion of the system when the block rocks around either the left corner A or the right corner B, have to be obtained. For the sake of brevity, in this section, only the relationships needed to describe the motion of system, when the block is rocking around left corner A are reported.

3.1.1 Equations of motion

The positions of mass centres of the bodies are evaluated with respect to an inertial reference frame with origin in O, initially coincident with the left base corner A of the block (Fig. 1a). The positions of mass centres G_1 and G_2 of the 2 d.o.f. structure are

$$x_{G1}(t) = \begin{Bmatrix} x_g(t) - d - d_G + u_1(t) \\ h_1 \\ 0 \end{Bmatrix}; \quad x_{G2}(t) = \begin{Bmatrix} x_g(t) - d - d_G + u_2(t) \\ h_2 \\ 0 \end{Bmatrix} \tag{1}$$

The position of the mass center C of the block during a rocking around the left corner A reads

$$x_C(t) = \begin{Bmatrix} x_g(t) \\ 0 \\ 0 \end{Bmatrix} + \begin{bmatrix} \mathrm{Cos}\vartheta(t) & -\mathrm{Sin}\vartheta(t) & 0 \\ \mathrm{Sin}\vartheta(t) & \mathrm{Cos}\vartheta(t) & 0 \\ 0 & 0 & 1 \end{bmatrix} \begin{Bmatrix} b \\ h_b \\ 0 \end{Bmatrix} \tag{2}$$

where the matrix is the rotation tensor of the block. The kinetic energy of the mechanical system during a rocking motion of the block around the left corner A reads

$$T = \frac{1}{2} \left[\sum_{i=1}^{2} m_i (\dot{x}_{Gi}(t) \cdot \dot{x}_{Gi}(t)) + J_C (\dot{\vartheta}(t) \cdot \dot{\vartheta}(t)) + M(\dot{x}_C(t) \cdot \dot{x}_C(t)) \right] \tag{3}$$

where m_1 and m_2 are the masses of the 2 d.o.f. system; $\vartheta(t) = \{0,\ 0,\ \dot{\vartheta}(t)\}^T$ and J_C is the polar inertia of the block with respect to its center of mass. In order to evaluate the potential energy for a rocking motion around the corner **A**, the distance vector between the couple of points W, K has to be evaluated. It is required to compute the potential energy associated to the elastic device with stiffness k_C. Such a distance vector reads

$$x_{WK}(t) = x_K(t) - x_W(t) = \begin{Bmatrix} d - Sin\vartheta(t)h_1 - u_1(t) \\ -h_1 + Cos\vartheta(t)h_1 \\ 0 \end{Bmatrix} \tag{4}$$

The potential energy of the system then read:

$$V = [Mg(x_C(t) - \bar{x}_C) \cdot j] + \frac{1}{2}\left[k_1(u_1(t))^2 + k_2\big(u_2(t) - u_1(t)\big)^2\right] + $$
$$\frac{1}{2}\left[k_C\big(\sqrt{x_{WK}(t) \cdot x_{WK}(t)} - d\big)^2\right] \tag{5}$$

where k_1 and k_2 are the stiffness of the 2 d.o.f. system; g is the gravity acceleration; $j = \{0,\ 1,\ 0\}^T$ is the unity vector of the y-axis; $\bar{x}_C = \{b,\ h_b,\ 0\}^T$ is the positions of the mass center corresponding to the minimum potential energy of the system. Since $\bar{x}_C$ in Eq. (5) is constant, it consequently plays no role in the derivation of the equations of motion.

The damping of the 2 d.o.f. system is modelled through two linear viscous dashpots with damping coefficients c_1 and c_2. The virtual work ∂W of the non-conservative viscous forces has to be considered to obtain the Lagrangian equations of motion; it reads

$$\partial W = -[c_1\dot{u}_1(t)\,\delta u_1(t) + c_2(\dot{u}_2(t) - \dot{u}_1(t))\,(\delta u_2(t) - \delta u_1(t))] \tag{6}$$

Finally, the equation of motion can be obtained by

$$\left[\frac{d}{dt}\left(\frac{\partial L}{\partial \dot{q}_i}\right) - \frac{\partial L}{\partial q_i}\right]\delta q_i = \delta W(\delta q_i), \forall \delta q_i \neq 0;\ (i = 1,2,3) \tag{7}$$

where $L = T - V$ is the Lagrangian function, $(q_1, q_2, q_3) = (u_1, u_2, \vartheta)$ and $(\delta q_1, \delta q_2,\ \delta q_3) = (\delta u_1, \delta u_2, \delta \vartheta)$. The equations of motion then read

$$-k_C(d - h_1\sin\vartheta - u_1)\frac{\left(\sqrt{d^2 - 2(d-u_1)h_1\sin\vartheta - 2du_1 - 2h_1{}^2\cos\vartheta + 2h_1^2 + u_1^2} - d\right)}{\sqrt{d^2 - 2(d-u_1)h_1\sin\vartheta - 2du_1 - 2h_1{}^2\cos\vartheta + 2h_1^2 + u_1^2}} +$$
$$(c_1 + c_2)\dot{u}_1 - c_2\dot{u}_2 + (k_1 + k_2)u_1 - k_2u_2 + m_1(\ddot{x}_g + \ddot{u}_1) = 0$$
$$- - - - - - - -$$
$$c_2(\dot{u}_2 - \dot{u}_1) + k_2(u_2 - u_1) + m_2(\ddot{x}_g + \ddot{u}_2) = 0 \tag{8}$$
$$- - - - - - - -$$
$$J_A\ddot{\vartheta} + \cos\vartheta\big(bgM - h_bM\ddot{x}_g\big) - M\sin\vartheta(b\ddot{x}_g + gh_b) +$$
$$k_Ch_1\big((u_1 - d)\cos\vartheta + h_1\sin\vartheta\big)\frac{\left(\sqrt{d^2 - 2(d-u_1)h_1\sin\vartheta - 2du_1 - 2h_1{}^2\cos\vartheta + 2h_1^2 + u_1^2} - d\right)}{\sqrt{d^2 - 2(d-u_1)h_1\sin\vartheta - 2du_1 - 2h_1{}^2\cos\vartheta + 2h_1^2 + u_1^2}} = 0$$

where J_A is the polar inertia of the block with respect to the right base corner A and the dependence on time t is removed to make the equation more readable. The equations of motion referring to a block that rocks around the right corner B can be obtained similarly. They are reported in Appendix 7.

3.1.2 Uplift and impact conditions of the block

The uplift conditions describe the initiation of rotation of the block. The uplift of the block around point A takes place when the resisting moment $M_R = Mgb$, due to the weight of the block gets smaller than the overturning moment $M_O = -M\ddot{x}_g(t)h_b + [k_C u_1(t)]h_1$ due to the inertial force and to the elastic one of the internal coupling device. All these moments are evaluated with respect to the base point A (Fig. 1(a)). By vanishing the sum of the two previous moments, it is possible to obtain the external acceleration $\ddot{x}_g$ able to uplift the block. Such an acceleration reads

$$\ddot{x}_g = \frac{g}{\lambda} + \frac{k_C u_1(t)h_1}{Mh_b} \tag{9}$$

where $\lambda = h_b/b$ is the slenderness of the block. In absence of the coupling with the device, the uplift condition is the same of a stand-alone block. The uplift condition around point B can be obtained similarly. It reported in Appendix 7.

During the rocking motion, when the rotation $\vartheta(t)$ approaches zero, an impact between the block and the ground occurs. Post-impact conditions of the rocking motion can be found assuming that the impact happens instantly, the body position remains unchanged and the angular momentum is maintained with respect to the base corner around which the block re-uplift after an impact. The post-impact angular velocity is equal to $\vartheta^+ = r\dot{\vartheta}^-$, where $r = (J_O - 2b\,S_y)/J_O$ is the restitution coefficient equal to that of stand-alone blocks (J_O is the polar inertia of the block with respect to one of the two base corners; $S_y = Mb$ is the static moment of the block with respect to a vertical axis passing through one of the two base corners). Experimental setup is arranged in such a way the block behaves as a perfectly rigid body. Some preliminary experimental tests have confirmed that the measured restitution coefficient of the block is very close to the analytical one. Specifically, the experimental restitution coefficient was obtained from some free rocking motion tests, performed on the stand-alone block, imposing different initial inclination of the block. The experimental restitution coefficient has been evaluated from the recorded time-histories of such rocking angle. The mean value of the ratio between the experimental restitution coefficient r_{exp} and the analytical one r_{th} is $r_{exp}/r_{th} = 0.992$. As an example, some experimental tests performed in Di Egidio *et al.* (2019a, 2015) confirm that the experimental and the analytical restitution coefficients can be very close to each other.

3.2 Experimental setup

The experimental investigation was performed in the laboratory Analytical, Numerical, Experimental Models for Civil Engineering (ANEMCE), which is a section of the Dynamics Laboratory of the Department of Civil, Architectural-Construction and Environmental Engineering (DICEAA) at University of L'Aquila, Italy.

Several challenging tasks were tackled in designing the coupling between the frame and the rigid block. The experimental setup consists of a two-storey frame and an aluminium rigid block, supported by a movable base driven by a long-stroke electromagnetic shaker (Fig. 2(a)). The shaker is an electromagnetic seismic simulator (EMSS) capable of testing scaled specimens. The rigid block stands over an adjustable base (Fig. 2(b)), sliding over two guides anchored to the base of the frame. The movable base is equipped with two sharpedged profiles which allow the block to rock without sliding, in order to avoid problems with the micro-sliding of the block as described in Kounadis (2018). The coupling spring is inserted in a thin rod, equipped with a hook on one side,

(a)

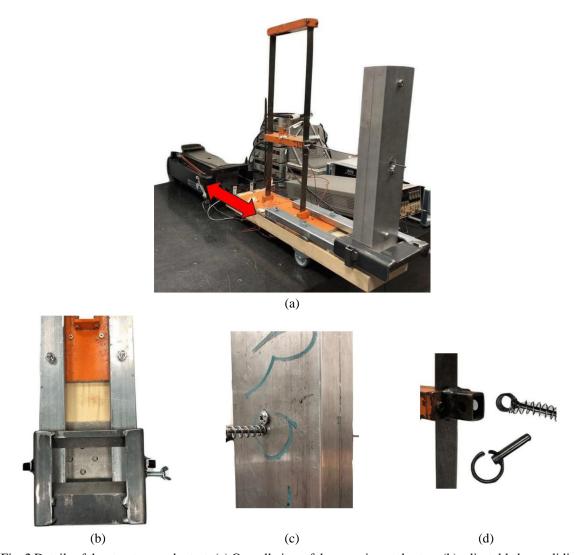(b)   (c)   (d)

Fig. 2 Details of the structure under test: (a) Overall view of the experimental setup; (b) adjustable base, sliding over two guides anchored to the base of the frame; (c) connection between the block and the spring (the spring is held by the head of a screw inserted in the rigid block); (d) connection between the first storey and the rigid block

avoiding instability of the spring under compression; the hooked end is locked with a catch on the first storey of the frame, while, on the other side, the rod is free to slide inside a flared hole, made in the center of mass of the block (Fig. 2(c)). The frictional force of the rod is made negligible by using lubricants, therefore in the analytical model, it is not considered. The spring is fixed on both the hook and the rigid block (Fig. 2(d)). The electrodynamic shaker is driven via a power control unit (amplifier) and the CompactRIO, a real-time embedded industrial controller made by National Instruments (NI). The CompactRIO is programmed in LabView in order to carry out both the harmonic analysis and the reproduction of time histories of recorded earthquakes. Two high-resolution Laser sensors (Micro-Epsilon optoNCDT 1420) are used as contact-free devices for

tracking the displacements of the two storeys. Measurements, observed via an oscilloscope and a spectrum analyser, were acquired by a NI acquisition board, which provides a sample rate up to 20000 samples/s and 14 bits resolution. A filter unit is implemented to cut off high frequencies induced by some overall noise. The recorded response is post-processed by means of the software MATLAB® and Mathematica®.

3.3 Parametric analysis

An extensive numerical and experimental parametric analysis is performed on the described mechanical system. The numerical integration of the equations of rocking motion Eq. (8) and Eq. (7.1), taking into account the uplift conditions Eq. (9) and Eq. (7.3) and the impact conditions, is performed by an original code developed by the same authors of this paper. The procedure is programmed to detect, from the first step of integration, the achievement of the uplift condition expressed by Eqs. (9) or (7.3). As long as these conditions are not verified, only the equations of motion for the sole 2-DOF are integrated. Then, once the block starts to uplift, according to Eq. (9) or (7.3), the algorithm starts with the integration of equation Eq. (8) for the rocking around the left corner A or Eq. (7.3) for the rocking around the right corner B, assuming as initial conditions for the 2-DOF, the values of u_1, u_2 and $\dot{u}_1, \dot{u}_2$ obtained at the end of the previous integration step.

After each integration step i, a check is made on the rocking angle ϑ. If $\vartheta_{t_{i-1}} * \vartheta_{t_i} < 0$, it means that an impact has occurred and the algorithm switches from a set of rocking equations to the other one by reducing the post-impact angular velocity $\dot{\vartheta}^+ = r\dot{\vartheta}^-$, as already explained in Section 3.1.2 - Uplift and impact conditions of the block. Moreover, at each step, a check is performed to verify if an overturning occurred. If so, the integration procedure is stopped. The classical four-order Runge-Kutta method is used as integration method. It is known that the search of the impact time has to be performed with a sufficient accuracy (Acikgoz *et al.* 2016, Diamantopoulos and Fragiadakis 2019). Therefore, the time step used in the numerical integration is $\Delta_t = 0.001s$, that assures a good accuracy in the evaluation of the times at which an impact occurs for harmonic excitation. Instead, for seismic excitation, a refined procedure has been adopted to find the time at which an impact occurs. Specifically, during the rocking motion, if in the successive integration time-step there is a change of sign of rocking angle, then algorithm re-start from the time before change of sign occurs and performs a further subdivision of the time-step in order to find the impact time with higher precision.

3.3.1 Frame and block characteristics
With reference to Fig. 1, the geometrical characteristics of the frame and of the block are shown in Table 1 and Table 2 respectively, whereas the mechanical characteristics of the system are shown in Table 3.

Table 1 Geometric characteristics of the the frame

Storeys	$h_1(m)$	$h_2(m)$
2	0.2	0.496

Table 2 Geometric characteristics of the the block

$2b(m)$	$2h_b(m)$	$s(m)$
0.05	0.4	0.10

Table 3 Mechanical characteristics of the 2 d.o.f. frame

k_1 (N/m)	k_2 (N/m)	m_1 (kg)	m_2 (kg)	ξ_1	ξ_2
213.44	56.45	1.062	1.062	0.010	0.035

In Table 3, ξ_1 and ξ_2 are the damping ratios of the 2 d.o.f. shear-type frame. All the quantities in Table 3 are directly measured (m_1 and m_2) or identified through preliminary free motion of the uncoupled frame (k_1, k_2, ξ_1 and ξ_2).

The mechanical characteristics of the frame have been chosen in order to have a highly deformable structure. This makes easy the observation of the motion during the experimental tests and its measurement. Specifically, the frequencies of the two oscillation modes of the stand-alone frame are: $f_1 \cong 1.0 Hz$ and $f_2 \cong 2.5 Hz$, thus confirming the high deformability of the system. The geometrical and mechanical characteristics of the block and of the connection have been chosen to enhance the dynamic response of the coupled system. As in Di Egidio *et al.* (2019d, 2020b), the spectral characteristics of the linearised coupled system, compared with those of the uncoupled one, is the main factor which affects the effectiveness of coupling. Therefore, in Section 4.1 - *Linearized equations,* the linearized equations will be used to interpret the working of coupled system.

3.3.2 Gain coefficient

The displacement u_1 and the drift $u_2 - u_1$ are used as indicators to evaluate the dynamic performance of the system. The smaller u_1 and $u_2 - u_1$ are, the greater the effectiveness of the coupling with the block is. As done in Fabrizio *et al.* (2017b), two gain parameters are then introduced

$$\alpha_1 = \frac{\max|u_1(t)|}{\max|\tilde{u}_1(t)|}, \quad \alpha_2 = \frac{\max|u_2(t)-u_1(t)|}{\max|\tilde{u}_2(t)-\tilde{u}_1(t)|} \tag{10}$$

where the displacements $\tilde{u}_1$ and $\tilde{u}_2$ refer to the uncoupled frame structure. If the parameters of Eq. (10) are less than unity, the coupling between the frame structure and the rocking block is beneficial for the frame structure.

This paper aims to study the effects of the coupling mainly on the part of the structure standing above the connecting point with the block (super-structure), that is described by the α_2 gain coefficient.

4. Harmonic analysis

The harmonic excitation used in the analyses is $\ddot{x}_g(t) = A_s \sin(\Omega t), 0 \le t \le t_{max}$, where A_s is the amplitude of the harmonic excitation and $t_{\max}$ is the maximum time used in the numerical integrations ($t_{\max} = 120s$). The high value of $t_{\max}$ is needed to reach stationary conditions. The comparison among numerical and experimental results is performed in stationary conditions since experimental tests manifested the following aspect: the steady-state response is highly repeatable, while the transient response suffers from repeatability issues. The structural system may exhibit significantly distinct transient responses to the same excitation, while approaching the almost identical steady-state response to that excitation. This fact remarks the significant effect of the initial conditions on the transient response. Due to dissipation, even in nonlinear systems, the effect of different initial conditions is lost when approaching the steady-state response if they all belong to

the same attracting basins.

The parameters considered in this analysis are the circular frequency of the harmonic excitation Ω and the coupling stiffness ratio $\beta = k_C/k_1$ (see Fig. 1(a)).

Since the mechanical system is nonlinear, its behaviour depends on the amplitude A_s of the excitation. In the analysis, a fixed value of the amplitude is taken. In fact, the amplitude is defined

$$A_s = 1.01g/\lambda \tag{11}$$

which is slightly greater than the uplift value of the stand-alone block. Since during the motion the rocking angle ϑ is always very small, the behaviour of the system is almost linear. It is observed that, for higher excitation amplitudes than the chosen one (up to a reasonable value), the response of the system is almost proportional to such excitation amplitude. Therefore, the excitation amplitude does not play an interesting role in the range of the investigated amplitude of the harmonic excitation.

4.1 Linearized equations

Linearized equations of motion need to be obtained for the correct interpretation of the results. These equations are based on the hypotheses of small rotations ϑ. The linearized equations of the coupled system can be obtained expanding the equations of motion in McLaurin series up to the first order, with respect to the Lagrangian parameters u_1, u_2 and ϑ. The equation of rocking motion around left corner read:

$$\mathbf{M}\ddot{\mathbf{X}} + \mathbf{K}\mathbf{X} = \mathbf{0} \tag{12}$$

where M is mass matrix, $\mathbf{X}$ is vector of Lagrangian parameters and $\mathbf{K}$ is stiffness matrix; by referring to the rocking motion of the block around the left base corner A, they read

$$\mathbf{M} = \begin{bmatrix} m_1 & 0 & 0 \\ 0 & m_2 & 0 \\ 0 & 0 & J_A \end{bmatrix}; \quad \mathbf{X} = \begin{Bmatrix} u_1 \\ u_2 \\ \vartheta \end{Bmatrix}$$

$$\mathbf{K} = \begin{bmatrix} k_1 + k_2 + k_C & -k_2 & h_1 k_C \\ -k_2 & k_2 & 0 \\ h_1 k_C & 0 & -h_b Mg + h_1{}^2 k_C \end{bmatrix} \tag{13}$$

The linearized equations of motion referring to the block that rocks around the right corner B are exactly equal to Eq. (12) and Eq. (13). Precisely, only the term J_A in the mass matrix M (Eq. (13)) change in J_B. However, due to the assumed symmetry of the block, it follows that $J_A = J_B$ (i.e., the polar inertia of the block around the two base corners are equal).

The frequencies and the modes of the coupled system are obtained by solving the following eigenproblem

$$(\mathbf{K} - \omega^2 \mathbf{M})\mathbf{\Psi} = 0 \tag{14}$$

where ω is the eigenvalue (linearized circular frequency) of the system and $\mathbf{\Psi}$ is the eigenvector (vibration mode).

In Fig. 3 the frequencies and the modal shapes (arrows) of the first and the second mode of both coupled and uncoupled system are reported. The third mode is not useful in the comprehension of the results since its frequency is very high and is out of the range of the investigated frequencies, therefore it is neglected in this paper.
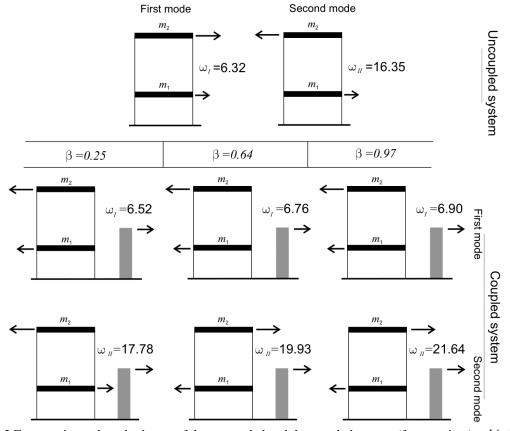
Fig. 3 Frequencies and mode shapes of the uncoupled and the coupled system (frequencies (rad/s^{-1})).

4.2 Numerical gain maps

In Fig. 4 the gain maps and surfaces of the coefficients α_1 and α_2 are shown. The surfaces in Fig. 4(a) represent the values of both gain coefficients in the parameter plane $\Omega - \beta$, obtained in stationary conditions. The maps, shown in Fig. 4(b), are the contour plots of the gain surfaces in the same parameter plane. In both the gain maps inside the light grey regions, α_1 and α_2 are less than unity. Hence, these regions, which are named gain region, represent combinations of the parameters for which the coupling with the rigid block is beneficial for the structure.

Particular attention is given to gain coefficient α_2, which represents the capability of the block to mitigate displacement of the super-structure. This means that through coupling with a rocking block a reduction of the drift of 80% can be achieved. Moreover, along the dash-dotted lines on the α_1 and α_2 maps the gain coefficients present the minimum value for each stiffness ratio β. This occurs for an excitation frequency $\Omega \cong 16.35 \; rad/s$ very close to the frequency of the second mode of the uncoupled system (see Fig. 3). Since in such a mode the two storeys of the frame structure move in counter phase, the drift of the super-structure is expected to be the higher possible. Instead, the same excitation frequency is sufficiently far from the frequencies of the second coupled mode. Then the displacements and the drift of the uncoupled system are greater than those of the coupled system, thus assuring gain coefficients less than unity.
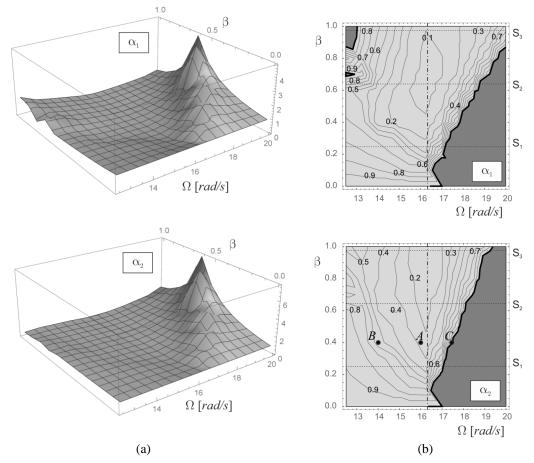
Fig. 4 Evaluation of the effectiveness of the coupling: (a) Gain surfaces of the coefficients α_1 and α_2; (b) Gain maps of the coefficient α_1 and α_2

Inside the dark grey region the coefficients α_1 and α_2 are greater than unity and no advantage from the coupling occurs. As can be observed in Fig. 4(a), the gain surfaces present points of relative maxima which move to higher frequencies when coupling stiffness increases. They are located in the dark grey region and can be explained as resonance conditions between the harmonic frequency and the frequency of the second coupled mode of the linearised system (see Fig. 3).

In order to investigate how the coupling works, the time-histories of coupled and uncoupled system are analysed. Fig. 5 shows the time-history of the drift $u_2 - u_1$ of both the coupled and the uncoupled system (left graphs) and of the displacement u_1 and the angle ϑ (right graphs). Both graphs in Fig. 5(a) refer to the point A in Fig. 4(b), which is located close to a relative minimum point of the α_2 gain surface. As can be observed, the time-history of the drift of the coupled system has a maximum amplitude smaller than the drift of the uncoupled system. Very interesting is the observation in the same graph of the time-histories of the displacement u_1 of the coupling storey and of the rocking angle ϑ. By taking into account the positive directions of the Lagrangian parameters (see Fig. 1(b)), the first storey and the block move almost in counter-phase. In such a case the block works as a Tuned Mass Damper for the structure.
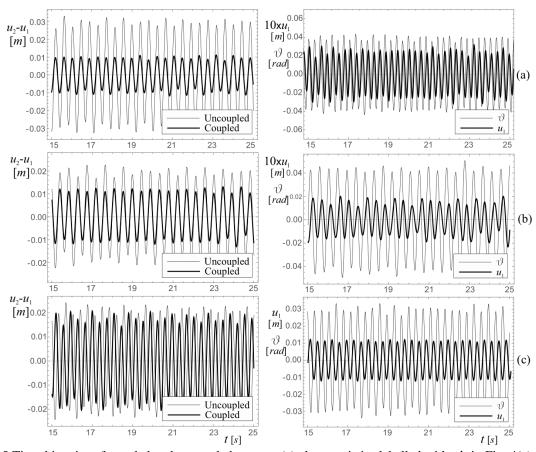
Fig. 5 Time-histories of coupled and uncoupled system: (a) characteristics labelled with A in Fig. 4(a) ($\Omega = 16; \beta = 0.4$); (b) characteristics labelled with B in Fig. 4(a) ($\Omega = 14; \beta = 0.4$); (c) characteristics labelled with C in Fig. 4(a) ($\Omega = 17.5; \beta = 0.4$)

    The time-histories of the point B (Fig. 5(b)), located in a point of the map where α_2 is greater than that in the point A, show a smaller reduction of the coupled drift than the uncoupled one. The observation of the evolution of u_1 and of ϑ highlights that the first storey and the block does not move in counter-phase, but neither in phase. As a consequence, there is a lower ability of the block to reduce the drift of the structure than the previous case. The time-histories of the point C (Fig. 5(c)), that is located very close to boundary of the gain region of the map in Fig. 4(b) (where $\alpha_2 = 1$), show a further worsening of the effectiveness of the coupling. In fact, the maximum amplitude of the drifts of the coupled and of the uncoupled systems are almost the same. On the contrary, the evolution of u_1 and ϑ show that in this case the first storey and the block move almost in phase, thus vanishing the effect of the coupling. It is worth observing that during the motion shown in Fig. 5(a), (b) the amplitude of the displacement u_1 is very small. In particular, it is much smaller than the amplitude of the rocking angle ϑ. In order to make u_1 clearly visible in the graphs where both u_1 and ϑ are reported (left graphs of Fig. 5(a), (b)), a scale factor equal to 10 is applied to the displacement u_1. In the motion shown in Fig. 5(c) it is not necessary to apply a scale factor to the displacement u_1 since it is of the same order of magnitude as the angle ϑ.
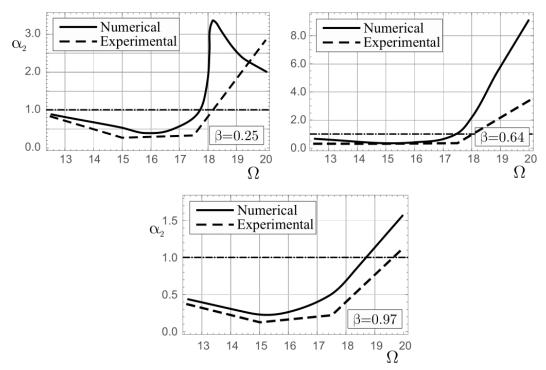
Fig. 6 Numerical and experimental α_2 gain spectra

4.3 Experimental gain spectra

Gain spectra provide the gain coefficients α_1 or α_2 versus the frequency of the harmonic excitation. They formally are sections for fixed β of the gain map (or of the gain surface), shown in Fig. 4. In the following section the interest will be focused on the sole α_2 gain spectrum.

Three experimental tests were performed, considering three different values of the coupling stiffness k_C (i.e., three values of β), in order to obtain three different gain spectra. The experimental results are compared with three corresponding sections of the gain map, labelled with S_1, S_2 and S_3 in Fig. 4. In order to obtain the experimental gain spectra, four different frequencies are considered for each value of the coupling stiffness; specifically $\Omega = 12.5, 15.0, 17.5$ and $20.0 rad/s$ are considered. During the tests, the time-histories of the total displacements u_1 and u_2 of both coupled and uncoupled system are acquired. The α_2 gain coefficient is the ratio of maximum drifts $u_2 - u_1$ of the coupled and uncoupled system, in stationary condition (after that the transient dynamics is vanished due to the damping of the system).

Fig. 6 shows three gain spectra, each one referring to different stiffness ratios β. Two different curves are reported in each graph. Solid line represents the gain spectrum obtained by the numerical integration of the mathematical model, whereas dashed line represents the gain spectrum obtained by the experimental investigation. It is useful remarking that the numerical curves (solid line) are section of the gain map in Fig. 4. Specifically, section S_1 refers to $\beta = 0.25$, section S_2 refers to $\beta = 0.64$, whereas section S_3 is obtained for $\beta = 0.97$.

The gain regions in each spectrum (the regions below the reference dash-dotted line passing through unity) are well described by the numerical results, since they are sufficiently close to the

experimental curves. However, outside the gain regions, the numerical results show a faster growth than that of the experimental ones. In particular, the numerical spectrum obtained for $\beta = 0.25$ (upper left graph) has a maximum at $\Omega \cong 18.0$. On the contrary, the experimental spectrum does not manifest a maximum in correspondence of the discrete values of the frequencies considered in the experiment ($12.5, 15.0, 17.5$ and $20\ rad/s$). For this maximum value the frequency of the excitation and the frequency of the second linearised coupled mode are close to each other ($\beta = 0.25$, Fig. 3). Since the excitation is almost in resonance condition with the second coupled mode, the displacements of such coupled system are higher than the displacements of the uncoupled one. For this reason the gain coefficient α_2 is higher than unity. In the other graphs, the numerical spectrum never reaches the resonance condition, since it is located outside the range of the considered frequencies Ω. In general, the growth that the experimental curves manifest outside the advantage region is slower than the numerical curves. This fact is possibly related to differences among the real and numerical frequencies of the second linearised mode, mainly due to imperfections of the real system. These imperfections can be identified in the small planarity defect of impacting surface and the not perfect symmetry of the block.

5. Seismic analysis

In order to check the validity of the analytical model and the performances of the coupling system, more complex excitations were selected. By thinking to a future use of such a method in Civil Engineering problems, in the numerical and experimental investigations a set of seven earthquake records is used as exciting input. Such seismic records have been selected to be sufficiently different to each other in terms of Peak Ground Acceleration (PGA), spectral content, length. The time histories, shown in Fig. 7, were opportunely scaled to have maximum PGA (Peak Groung Acceleration) 20% higher than the uplift acceleration of the stand-alone block. The earthquake records are fully listed below:

1. Pacoima, Dam-164 ground motion recorded during the 1971 San Fernando, California earthquake;
2. Parkfield, CO2-065 ground motion recorded during the California earthquake 1966;
3. Erzincan, NS ground motion recorded during the 1992 Turkey earthquake;
4. El Centro, CA - Array Sta 9 - Imperial Valley Irrigation District - 302 Commercial (component 180), 1979;
5. L'Aquila, IT.AQV.HNE.D.20090406.013240.X.ACC station, ground motion recorded during the 2009 Italian earthquake;
6. Newhall, Newhall-360 station, ground motion recorded during the 1994 Northridge, California earthquake;
7. Kobe, Takarazuka-000 station, ground motion recorded during the 1995 Japan earthquake.

5.1 Analytical and experimental results

Gain curves, providing the value of the α_2 gain coefficient versus the stiffness ratio β, are obtained. The experimental curves are derived by considering three different values of the stiffness ratio β (the same used in the harmonic analysis) for each earthquake. Although the experimental tests have been performed by selecting only three values of the coupling stiffness (β), the experimental gain curves have been obtained approximately by connecting these few points. Then,
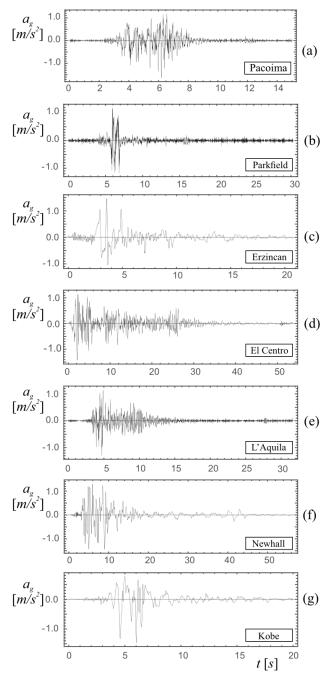
Fig. 7 Time histories of the earthquakes analysed: (a) Pacoima; (b) Parkfield; (c) Erzincan; (d); El Centro; (e) L'Aquila; (f) Newhall; (g) Kobe

the experimental curves are compared with the numerical ones. During the numerical and the experimental tests, the time-histories of the total displacements u_1 and u_2 of both coupled and uncoupled system are acquired.
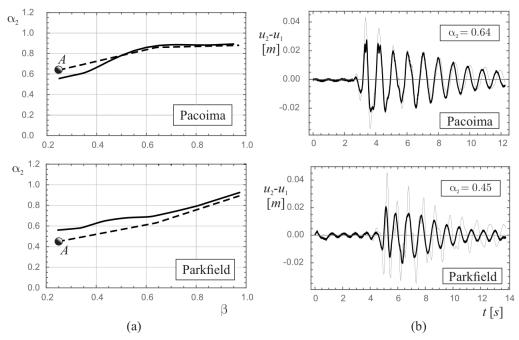
Fig. 8 Seismic analysis: (a) Experimental (dashed line) and analytical (solid line) gain curves of two different earthquakes Pacoima (top) and Parkfield (bottom); (b) Experimental time-histories of super-structure drift of the uncoupled (thin line) and the coupled (thick line) structure, related to points A ($\beta = 0.25$)

Specifically, for the two earthquakes Pacoima (Fig. 7(a)) and Parkfield (Fig. 7(b)), a comparison between analytical and experimental models is performed. In Fig. 8(a) the numerical and the experimental gain curves are reported, whereas Fig. 8(b) shows the experimental time-histories of the super-structure drift. As can be observed, the numerical and the experimental gain curves for both the earthquakes match well, assuring the good quality of the analytical model and of the results. Moreover, since for both earthquakes the α_2 gain coefficient is always less than unity, the coupling with the rigid block is beneficial for the frame structure. The best behaviour of the coupling, that corresponds to smaller values of α_2, occurs mainly for smaller values of the coupling stiffness. In fact, for higher values of the stiffness ratio β, the gain curves approach the unity. The comparison between the time-histories of the drift of the uncoupled and the coupled systems, both referring to point A in Fig. 8(a) ($\beta = 0.25$), shows the sensible reduction of the oscillation amplitudes of the coupled system with respect to the uncoupled one.

To conclude, the proposed comparisons among numerical and experimental results are judged to be able to validate correctly the analytical model. Other (exclusively) numerical results referring to the other five earthquake records, will be used in the next Section. They have the aim to check the effectiveness of coupling with a rocking wall under different seismic excitations, to be sure that the system is able to work well in different conditions.

5.2 Experimental gain curves

Experimental seismic investigations using the other five earthquakes Erzincan, El Centro, L'Aquila, Newall, and Kobe (from Fig. 7(c) to Fig. 7(g), respectively) are performed. In Fig. 9(a),
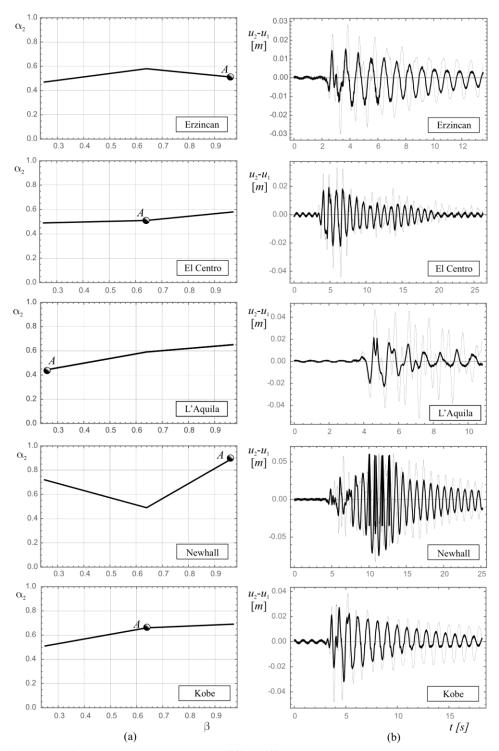
Fig. 9 Seismic analysis: (a) Experim. gain curves of five different earthquakes; (b) Experimental time-histories of the super-structure drift of the uncoupled (thin line) and the coupled (thick line) structure related to points *A*, labelled to the relevant gain curves

the experimental gain curve of the five different earthquakes are shown.

In all the cases, the gain coefficient α_2 is less than unity, assuring beneficial effects in reduction of the drift of the super-structure. As can be observed, through the coupling with a rocking block, it is possible to reach around the 50% drift reduction. The minimum value of α_2 is obtainable in each earthquake, for a different value of β; hence the choice of the characteristics of block and coupling device is a fundamental aspect, in order to obtain the best performances of the coupled system. Finally, the time histories of the drift of the coupled and uncoupled system, referring to point *A* of the relevant gain curves, are shown in Fig. 9(b). They all confirm the results reported by the gain curves and the strong effect of coupling the frame structure to a rigid block.

6. Conclusions

A 2 d.o.f. shear-type frame is elastically coupled with an aluminum rocking block to improve the dynamics of the system. Both the frame and the block have fixed characteristics, whereas the stiffness of the coupling device was considered as variable parameter. The non-linear equations of motion were obtained by a Lagrangian approach and successively numerically integrated to analyze the behaviour of the coupled system. The coupling with the block improves the behaviour of the frame structure in terms of displacements. Simulations were performed considering both harmonic and seismic excitation. The results were summarized in gain curves, maps and several gain spectra plotted in the system's parameters plane. In the harmonic analysis, characterizing parameters are the frequency of the harmonic excitation and the stiffness of the coupling device. The gain map provides the ratio of the maximum displacement or drift of the coupled and the uncoupled systems. When this ratio is less than unity, the coupling with the block enhances the dynamics of the frame structure. Results have shown the existence of a significant advantage region in the parameters plane, where the coupling is beneficial for the system. Experimental simulations are aimed at validating the results of the analytical model. The same mechanical system, studied in numerical simulations, was experimentally tested using a harmonically driven electro-dynamic long-stroke shaker. The response of the experimental system, arranged in gain spectra (i.e. sections of the previous gain map), were compared with the numerical sections. The comparison confirms the effectiveness of the analytical model in predicting the actual behaviour of the experimental system. Further, it gives an affirmation of the capability of the rigid rocking block in improving the response of the frame system. In order to check the validity of the analytical model and the performances of the coupling system under more complex excitations, seven registered earthquakes were selected. In this analysis, only stiffness of the coupling device was considered as a parameter. The numerical and experimental results of two earthquakes were compared to each other, confirming the validity of the analytical model and the sound efficiency of the coupling. The experimental tests performed by using the other five earthquakes confirm an improvement of the behaviour of the coupled frame with respect to the uncoupled one.

References

Acikgoz, S., Ma, Q., Palermo, A. and DeJong, M. (2016), "Experimental identification of the dynamic characteristics of a flexible rocking structure", *J. Earthq. Eng.*, **20**(8), 1199-1221. https://doi.org/10.1080/13632469.2016.1138169.

Aghagholizadeh, M. and Makris, N. (2018), "Earthquake response analysis of yielding structures coupled with vertically restrained rocking walls", *Earthq. Eng. Struct. Dyn.*, **47**(15), 2965-2984. https://doi.org/10.1002/eqe.3116.

Aloisio, A., Alaggio, R. and Fragiacomo, M. (2019a), "Dynamic identification of a masonry facade from seismic response data based on an elementary Ordinary Least Squares approach", *Eng. Struct.*, **197**, 109415. https://doi.org/10.1016/j.engstruct.2019.109415.

Aloisio, A., Antonacci, E., Fragiacomo, M. and Alaggio, R. (2020), "The recorded seismic response of the Santa Maria di Collemaggio basilica to low-intensity earthquakes", *Int. J. Arch. Heritage*, 1-19. https://doi.org/10.1080/15583058.2020.1802533.

Aloisio, A., Di Battista, L., Alaggio, R. and Fragiacomo, M. (2019b), "Analysis of the forced dynamics of a masonry facade by means of input-output techniques and a linear regression model", *COMPDYN 2019, 7th International Conference on Computational Methods in Structural Dynamics and Earthquake Engineering*.

Andreaus, U. (1990), "Sliding-uplifting response of rigid blocks to base excitation", *Earthq. Eng. Struct. Dyn.*, **19**(8), 1181-1196. https://doi.org/10.1002/eqe.4290190808.

Brzeski, P., Kapitaniak, T. and Perlikowski, P. (2016), "The use of tuned mass absorber to prevent overturning of the rigid block during earthquake", *Int. J. Struct. Stab. Dyn.*, **6**(10), Article ID 1550075. https://doi.org/10.1142/S0219455415500753.

Caliò, I. and Marletta, M. (2003), "Passive control of the seismic response of art objects", *Eng. Struct.*, **25**, 1009-1018. https://doi.org/10.1016/S0141-0296(03)00045-2.

Ceravolo, R., Pecorelli, M. and Zanotti Fragonara, L. (2016), "Semi-active control of the rocking motion of monolithic art objects", *J. Sound Vib.*, **374**, 1-16. https://doi.org/10.1016/j.jsv.2016.03.038.

Ceravolo, R., Pecorelli, M. and Zanotti Fragonara, L. (2017), "Comparison of semi-active control strategies for rocking objects under pulse and harmonic excitations", *Mech. Syst. Signal Pr.*, **90**, 175-188. https://doi.org/10.1016/j.ymssp.2016.12.006.

Collini, L., Garziera, R., Riabova, K., Munitsyna, M. and Tasora, A. (2016), "Oscillations control of rocking-block-type buildings by the addition of a tuned pendulum", *Shock Vib.*, **2016**, Article ID 8570538. https://doi.org/10.1155/2016/8570538.

Contento, A. and Di Egidio, A. (2009), "Investigations into benefits of base isolation for NonSymmetric rigid blocks", *Earthq. Eng. Struct. Dyn.*, **38**, 849-866.

Contento, A. and Di Egidio, A. (2014), "On the use of base isolation for the protection of rigid bodies placed on a multi-storey frame under seismic excitation", *Eng. Struct.*, **62-63**, 1-10. https://doi.org/10.1016/j.engstruct.2014.01.019.

Contento, A., Gardoni, P., Di Egidio, A. and de Leo, A. (2017), "Probabilistic models to assess the seismic safety of rigid block-like structures and the effectiveness of two safety devices", *Procedia Eng.*, **199**(2017), 1164-1169. https://doi.org/10.1061/(ASCE)ST.1943-541X.0002431.

Contento, A., Gardoni, P., Di Egidio, A. and de Leo, A. (2019), "Probabilistic models to assess the seismic safety of rigid block-like elements and the effectiveness of two safety devices", *J. Struct. Eng.*, **145**(11), 04019133. https://doi.org/10.1061/(ASCE)ST.1943-541X.0002431.

Corbi, O. (2006), "Laboratory investigation on sloshing water dampers coupled to rigid blocks with unilateral constraints", *Int. J. Mech. Solid.*, **1**(1), 29-40.

Dar, A., Konstantinidis, D. and ElDakhakhni, W. (2018), "Seismic response of rocking frames with top support eccentricity", *Earthq. Eng. Struct. Dyn.*, **47**(12), 2496-2518. https://doi.org/10.1002/eqe.3096.

de Leo, A., Simoneschi, G., Fabrizio, C. and Di Egidio, A. (2016), "On the use of a pendulum as mass damper to control the rocking motion of a non-symmetric rigid block", *Meccanica*, **51**, 2727-2740. https://doi.org/10.1007/s11012-016-0448-5.

DeJong, M. and Dimitrakopoulos, E. (2014), "Dynamically equivalent rocking structures", *Earthq. Eng. Struct. Dyn.*, **43**(10), 1543-1563. https://doi.org/10.1002/eqe.2410.

Di Egidio, A. and Contento, A. (2009), "Base isolation of sliding-rocking non-symmetyric rigid blocks subjected to impulsive and seismic excitations", *Eng. Struct.*, **31**, 2723-2734.

Di Egidio, A. and Contento, A. (2010), "Seismic response of a non-symmetric rigid block on a constrained oscillating base", *Eng. Struct.*, **32**, 3028-3039. https://doi.org/10.1016/j.engstruct.2010.05.022.

Di Egidio, A., Alaggio, R., Aloisio, A., de Leo, A., Contento, A. and Tursini, M. (2019a), "Analytical and experimental investigation into the effectiveness of a pendulum dynamic absorber to protect rigid blocks from overturning", *Int. J. Nonlin. Mech.*, **115**, 1-10. https://doi.org/10.1016/j.ijnonlinmec.2019.04.011.

Di Egidio, A., Alaggio, R., Contento, A., Tursini, M. and Della Loggia, E. (2015), "Experimental characterization of the overturning of three-dimensional square based rigid block", *Int. J. Nonlin. Mech.*, **69**, 137-145. https://doi.org/10.1016/j.ijnonlinmec.2014.12.003.

Di Egidio, A., Contento, A., Fabrizio, C. and de Leo, A. (2019b), "Visco-elastic coupling between a linear two-dof system and a rocking rigid block to improve the dynamic response", *J. Phys.: Conf. Ser.*, **1264**(2019), 012029.

Di Egidio, A., Contento, A., Olivieri, C. and de Leo, A. (2020a), "Protection from overturning of rigid block-like objects with Linear Quadratic Regulator active control", *Struct. Control Hlth Monit.*, **27**, e2598. https://doi.org/10.1002/stc.2598.

Di Egidio, A., de Leo, A. and Contento, A. (2019c), "The use of a pendulum dynamic mass absorber to protect a trilithic symmetric system from the overturning", *Math. Prob. Eng.*, **2019**, Article ID 4843738, 14. https://doi.org/10.1155/2019/4843738.

Di Egidio, A., de Leo, A. and Simoneschi, G. (2018), "Effectiveness of mass-damper dynamic absorber on rocking block under one-sine pulse ground motion", *Int. Limit. Nonlin. Mech.*, **98**, 154-162. https://doi.org/10.1016/j.ijnonlinmec.2017.10.015.

Di Egidio, A., Pagliaro, S., Fabrizio, C. and de Leo, A. (2019d), "Dynamic response of a linear two d.o.f system visco-elastically coupled with a rigid block", *Coupl. Syst. Mech.*, **8**(4), 351-375. https://doi.org/10.12989/csm.2019.8.4.351.

Di Egidio, A., Pagliaro, S., Fabrizio, C. and de Leo, A. (2020b), "Seismic performance of frame structures coupled with an external rocking wall", *Eng. Struct.*, **224**, 111207. https://doi.org/10.1016/j.engstruct.2020.111207.

Di Egidio, A., Simoneschi, G., Olivieri, C. and de Leo, A. (2014a), "Protection of slender rigid blocks from the overturning by using an active control system", *Proceedings of the XXIII Conference The Italian Association of Theoretical and Applied Mechanics*.

Di Egidio, A., Zulli, D. and Contento, A. (2014b), "Comparison between the seismic response of 2D and 3D models of rigid blocks", *Earthq. Eng. Eng. Vib.*, **13**, 151-162. https://doi.org/10.1007/s11803-014-0219-z.

Diamantopoulos, S. and Fragiadakis, M. (2019), "Seismic response assessment of rocking systems using single degreeoffreedom oscillators", *Earthq. Eng. Struct. Dyn.*, **48**(7), 689-708. https://doi.org/10.1002/eqe.3157.

Dimitrakopoulos, E. and DeJong, M. (2012), "Overturning of retrofitted rocking structures under pulse-type excitations", *J. Eng. Mech.*, **138**, 963-972. https://doi.org/10.1061/(ASCE)EM.1943-7889.0000410.

Fabrizio, C., de Leo, A. and Di Egidio, A. (2017a), "Structural disconnection as a general technique to improve the dynamic and seismic response of structures: a basic model", *Procedia Eng.*, **199**, 1635-1640. https://doi.org/10.1016/j.proeng.2017.09.086.

Fabrizio, C., de Leo, A. and Di Egidio, A. (2019), "Tuned mass damper and base isolation: a unitary approach for the seismic protection of conventional frame structures", *J. Eng. Mech.*, **145**(4), 04019011. https://doi.org/10.1061/(ASCE)EM.1943-7889.0001581.

Fabrizio, C., Di Egidio, A. and de Leo, A. (2017b), "Top disconnection versus base disconnection in structures subjected to harmonic base excitation", *Eng. Struct.*, **152**, 660-670. https://doi.org/10.1016/j.engstruct.2017.09.041.

Grigorian, C. and Grigorian, M. (2015), "Performance control and efficient design of rocking-wall moment frames", *J. Struct. Eng.*, **142**(2), 04015193. https://doi.org/10.1061/(ASCE)ST.1943-541X.0001411.

Housner, G. (1963), "The behavior of inverted pendulum structures during earthquakes", *Bull. Seismol. Soc. Am.*, **53**(2), 404417.

Huang, W., McClurea, G. and Hussainzadab, N. (2013), "Seismic interactions between suspended ceilings and nonstructural partition walls", *Coupl. Syst. Mech.*, **2**(4), 329-348. https://doi.org/10.12989/csm.2013.2.4.329.

Kalliontzis, D., Sritharan, S. and Schultz, A. (2016), "Improved coefficient of restitution estimation for free

rocking members", *J. Struct. Eng.*, **142**, 06016002. https://doi.org/10.1061/(ASCE)ST.1943-541X.0001598.

Khatiwada, S., Nawawi and Chouw, N. (2013), "A shake table investigation on interaction between buildings in a row", *Coupl. Syst. Mech.*, **2**(2), 175-190. https://doi.org/10.12989/csm.2013.2.2.175.

Kounadis, A. (2014), "Rocking instability of free-standing statues atop slender viscoelastic columns under ground motion", *Soil Dyn. Earthq. Eng.*, **63**(9), 83-91. https://doi.org/10.1016/j.soildyn.2014.01.021.

Kounadis, A. (2015), "New findings in the rocking instability of one and two rigid block systems under ground motion", *Meccanica*, **50**(9), 2219-2238. https://doi.org/10.1007/s11012-015-0167-3.

Kounadis, A. (2018), "The effect of sliding on the rocking instability of multi-rigid block assemblies under ground motion", *Soil Dyn. Earthq. Eng.*, **104**, 1-14. https://doi.org/10.1016/j.soildyn.2017.03.035.

Kounadis, A.N. (2013), "Parametric study in rocking instability of a rigid block under harmonic ground pulse: a unified approach", *Soil Dyn. Earthq. Eng.*, **45**, 125143. https://doi.org/10.1016/j.soildyn.2012.10.002.

Makris, N. and Aghagholizadeh, M. (2017), "The dynamics of an elastic structure coupled with a rocking wall", *Soil Dyn. Earthq. Eng.*, **46**, 945-954. https://doi.org/10.1002/eqe.2838.

Makris, N. and Zhang, J. (2001), "Rocking response of anchored blocks under pulse-type motions", *J. Eng. Mech.*, **127**(5), 484-493. https://doi.org/10.1061/(ASCE)0733-9399(2001)127:5(484).

Muratovi, A. and Ademovi, N. (2015), "Influence of masonry infill on reinforced concrete frame structures seismic response", *Coupl. Syst. Mech.*, **4**(2), 173-189. http://dx.doi.org/10.12989/csm.2015.4.2.173.

Ormeo, M., Tam Larkin, T. and Chouw, N. (2012), "Influence of uplift on liquid storage tanks during earthquakes", *Coupl. Syst. Mech.*, **1**(4), 311-324. http://dx.doi.org/10.12989/csm.2012.1.4.311.

Pompei, A., Scalia, A. and Sumbatyan, M. (1998), "Dynamics of rigid block due to horizontal ground motion", *J. Eng. Mech.*, **124**(7), 713-717. https://doi.org/10.1061/(ASCE)0733-9399(1998)124:7(713).

Psycharis, I.N., Fragiadakis, M. and Stefanou, I. (2013), "Seismic reliability assessment of classical columns subjected to nearfault ground motions", *Earthq. Eng. Struct. Dyn.*, **42**(14), 2061-2079. https://doi.org/10.1002/eqe.2312.

Shenton, H. (1996), "Criteria for initiation of slide, rock, and slide-rock rigid-body modes", *J. Eng. Mech.*, **122**(7), 690-693. https://doi.org/10.1061/(ASCE)0733-9399(1996)122:7(690).

Shenton, H. and Jones, N. (1991), "Base excitation of rigid bodies. I: Formulation", *J. Eng. Mech.*, **117**(10), 2286-2306. https://doi.org/10.1061/(ASCE)0733-9399(1991)117:10(2286).

Simoneschi, G., de Leo, A. and Di Egidio, A. (2017a), "Effectiveness of oscillating mass damper system in the protection of rigid blocks under impulsive excitation", *Eng. Struct.*, **137**, 285-295. https://doi.org/10.1016/j.engstruct.2017.01.069.

Simoneschi, G., Geniola, A., de Leo, A. and Di Egidio, A. (2017b), "On the seismic performances of rigid blocks coupled with an oscillating mass working as TMD", *Earthq. Eng. Struct. Dyn.*, **46**, 1453-1469. https://doi.org/10.1002/eqe.2864.

Simoneschi, G., Olivieri, C., de Leo, A. and Di Egidio, A. (2018), "Pole placement method to control the rocking motion of rigid blocks", *Eng. Struct.*, **167**, 39-47. https://doi.org/10.1016/j.engstruct.2018.04.016.

Sorrentino, L., AlShawa, O. and Decanini, L. (2011), "The relevance of energy damping in unreinforced masonry rocking mechanisms. Experimental and analytic investigations", *Bull. Earthq. Eng.*, **9**(5), 1617-1642. https://doi.org/10.1007/s10518-011-9291-1.

Spanos, P. and Koh, A. (1984), "Rocking of rigid blocks due to harmonic shaking", *J. Eng. Mech.*, **110**, 1627-1642. https://doi.org/10.1061/(ASCE)0733-9399(1984)110:11(1627).

Spanos, P. and Koh, A. (1986), "Analysis of block random rocking", *Soil Dyn. Earthq. Eng.*, **5**, 178-183. https://doi.org/10.1016/0267-7261(86)90021-7.

Spanos, P., Di Matteo, A., Pirrotta, A. and Di Paola, M. (2017), "Rocking of rigid block on nonlinear flexible foundation", *Int. J. Nonlin. Mech.*, **94**, 362-374. https://doi.org/10.1016/j.ijnonlinmec.2017.06.005.

Taniguchi, T. (2002), "Non-linear response analyses of rectangular rigid bodies subjected to horizontal and vertical ground motion", *Earthq. Eng. Struct. Dyn.*, **31**, 1481-1500. https://doi.org/10.1002/eqe.170.

Ther, T. and Kollar, L. (2016), "Refinement of Housners model on rocking blocks", *Bull. Earthq. Eng.*, **15**, 2305-2319. https://doi.org/10.1016/S0267-7261(02)00115-X.

Tung, C. (2007), "Initiation of motion of a free-standing body to base excitation", *Earthq. Eng. Struct. Dyn.*, **36**, 1431-1439. https://doi.org/10.1002/eqe.703.

Vassiliou, M. and Makris, N. (2012), "Analysis of the rocking response of rigid blocks standing free on a seismically isolated base", *Earthq. Eng. Struct. Dyn.*, **41**(2), 177-196. https://doi.org/10.1002/eqe.1124.

Vassiliou, M., K.R., M. and Stojadinovi, B. (2014), "Dynamic response analysis of solitary flexible rocking bodies: modeling and behavior under pulselike ground excitation", *Earthq. Eng. Struct. Dyn.*, **43**(10), 1463-1481. https://doi.org/10.1002/eqe.2406.

Voyagaki Ioannis, E., Psycharis, I. and Mylonakis, G. (2013), "Rocking response and overturning criteria for free standing rigid blocks to singlelobe pulses", *Soil Dyn. Earthq. Eng.*, **46**, 85-95. https://doi.org/10.1016/j.soildyn.2012.11.010.

Wada, A., Qu, Z., Motoyui, S. and Sakata, H. (2011), "Seismic retrofit of existing SRC frames using rocking walls and steel dampers", *Front. Arch. Civil Eng. China*, **5**(3), 259266. https://doi.org/10.1007/s11709-011-0114-x.

Yim, C., Chopra, A. and Penzien, J. (1980), "Rocking response of rigid blocks to earthquakes", *Earthq. Eng. Struct. Dyn.*, **438**(6), 565-587. https://doi.org/10.1002/eqe.4290080606.

Zhang, J. and Makris, N. (2001), "Rocking response of free-standing blocks under cycloidal pulses", *J. Eng. Mech.*, **127**(5), 473-483. https://doi.org/10.1061/(ASCE)0733-9399(2001)127:5(473).

Zulli, D., Contento, A. and Di Egidio, A. (2012), "Three-dimensional model of rigid block with a rectangular base subject to pulse-type excitation", *Int. J. Nonlin. Mech.*, **47**, 679-687. https://doi.org/10.1016/j.ijnonlinmec.2011.11.004.

IA

Appendix A. Rocking of the block around the right corner

The equations of motion of the system when the block rocks around the right corner B read

$$
k_C(-2b - d + 2b\cos\vartheta + h_1\sin\vartheta + u_1)\frac{(\sqrt{Terms_1}-d)}{\sqrt{Terms_1}} +
$$
$$
(c_1 + c_2)\dot{u}_1 - c_2\dot{u}_2 + (k_1 + k_2)u_1 - k_2 u_2 + m_1(\ddot{x}_g + \ddot{u}_1) = 0
$$
$$

$$
$$
c_2(\dot{u}_2 - \dot{u}_1) + k_2(u_2 - u_1) + m_2(\ddot{x}_g + \ddot{u}_2) = 0 \qquad\qquad\text{(A.1)}
$$
$$

$$
$$
J_B\ddot{\vartheta} - \cos\vartheta(bgM + h_b M\ddot{x}_g) + M\sin\vartheta(b\ddot{x}_g - gh_b) +
$$
$$
k_C(h_1(u_1 - d)\cos\vartheta + (h_1^2 + 2b(2b + d - u_1))\sin\vartheta)\frac{(\sqrt{Terms_1}-d)}{\sqrt{Terms_1}} = 0
$$

where

$$
Terms_1 = 8b^2 - 4b(2b + d)\cos(\vartheta(t)) + u_1(t)\left(4b\cos(\vartheta(t)) - 4b - 2d + u_1(t)\right) +
$$
$$
4bd + d^2 + 2h_1(u_1(t) - d)\sin(\vartheta(t)) - 2h_1^2(\cos(\vartheta(t)) - 1) \qquad\text{(A.2)}
$$

The uplift condition around the right corner B reads

$$
\ddot{x}_g = -\frac{g}{\lambda} + \frac{k_C u_1(t)h_1}{Mh_b} \qquad\qquad\text{(A.3)}
$$